iScience

CellPress
OPEN ACCESS

Article

Single-cell RNA sequencing reveals epithelial cells driving brain metastasis in lung adenocarcinoma

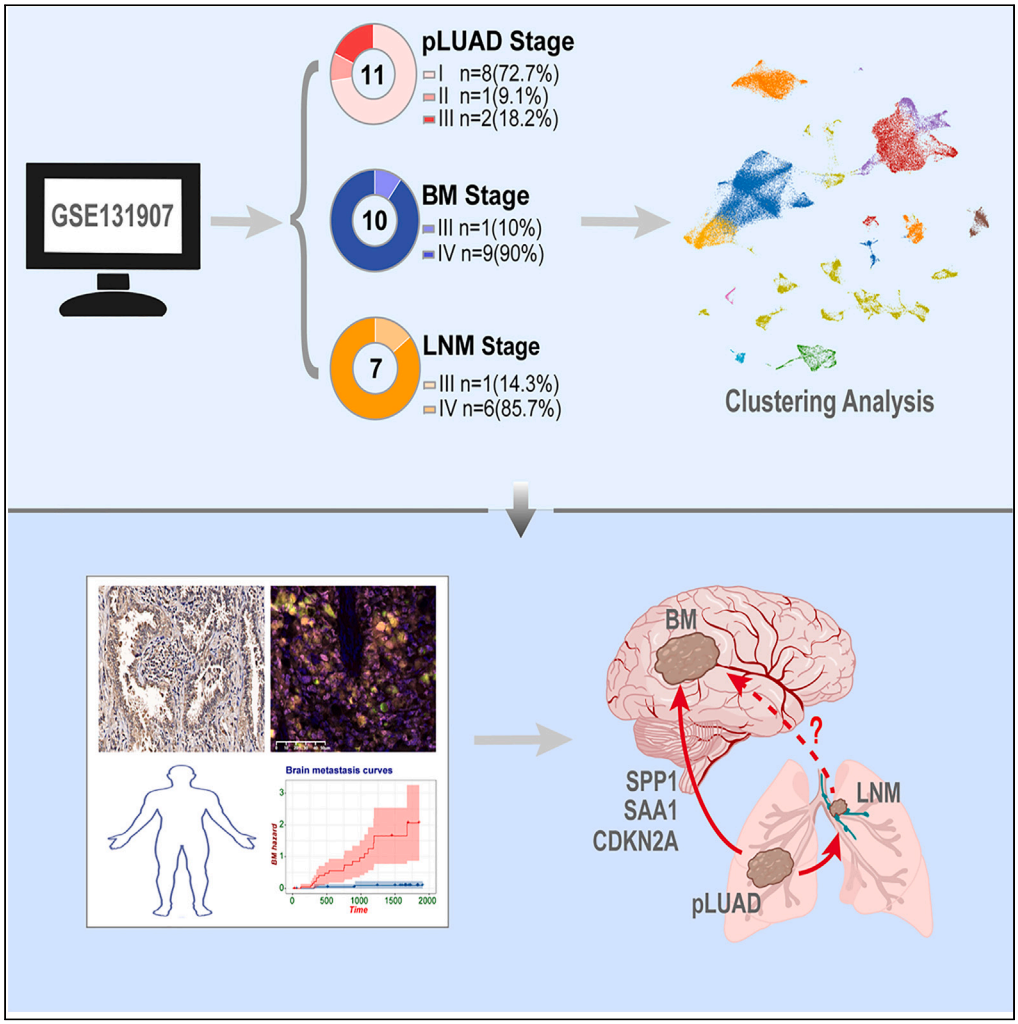

Yonghui Wu, Fujun Yang, Shilan Luo, ..., Yajuan Cao, Lixin Wang, Xiao Song

dr_caoy@aliyun.com (Y.C.)
1701005@tongji.edu.cn (L.W.)
songxiao198327@163.com (X.S.)

Highlights

Distinct cell components between primary lung adenocarcinoma and brain metastasis (BM)

The association between BM and lymph node metastasis (LNM) lesions may be indirect

Aneuploid cells of brain metastasis-associated epithelial cells were associated with BM

Wu et al., iScience 27, 109258
March 15, 2024
https://doi.org/10.1016/j.isci.2024.109258

iScience

CellPress
OPEN ACCESS

Article

Single-cell RNA sequencing reveals epithelial cells driving brain metastasis in lung adenocarcinoma

Yonghui Wu,[1,2,5] Fujun Yang,[3,5] Shilan Luo,[4,5] Xiang Li,[3] Zhan Gu,[1] Rui Fan,[1] Yajuan Cao,[1,*] Lixin Wang,[1,*] and Xiao Song[3,6,*]

SUMMARY

Brain metastases (BM) of lung adenocarcinoma (LUAD) are the most common intracranial malignancy leading to death. However, the cellular origins and drivers of BM from LUAD have not been clarified. Cellular composition was characterized by single-cell sequencing analysis of primary lung adenocarcinoma (pLUAD), BM and lymph node metastasis (LNM) samples in GSE131907. Our study briefly analyzed the tumor microenvironment (TME), focusing on the role of epithelial cells (ECs) in BM. We have discovered a population of brain metastasis-associated epithelial cells (BMAECs) expressing SPP1, SAA1, and CDKN2A, and it has been observed that this population is mainly composed of aneuploid cells from pLUAD, playing a crucial role in brain metastasis. Our study concluded that both LNM and BM in LUAD originated from pLUAD lesions, but there is currently insufficient evidence to prove a direct association between BM lesions and LNM lesions, which provides inspiration for further investigation of the TME in BM.

INTRODUCTION

Lung adenocarcinoma (LUAD) is the most common type of non-small-cell lung cancer (NSCLC),[1] and approximately 25% of patients with LUAD would eventually develop brain metastases (BM).[2] Unfortunately, patients diagnosed with brain metastasis from lung cancer presented a poor prognosis. The brain microenvironment has unique cell types, anatomical structures, metabolic restrictions, and immune environment, which differs significantly from the microenvironment of extracranial lesions.[3,4] Treatment options for brain metastasis from lung cancer are limited, which include surgical resection, radiotherapy, and systemic treatment targeting the primary lung adenocarcinoma (pLUAD). Regrettably, these therapeutic approaches failed to yield satisfactory outcomes.[5,6] Therefore, early identification of patients at high risk of BM from LUAD and the development of targeted drugs are particularly important.

Recently, with the popularity of tumor immunotherapy and targeted therapy,[7,8] more scholars pay attention to the impact of the interaction between immune cells and tumor cells in the microenvironment, as well as the development of RNAi drugs.[9] There have been many studies, which mainly focused on the application of transcriptome and proteomic sequencing, were carried out to screen biomarkers to predict BM occurrence and explore the molecular mechanism of BM development.[10] The PI3K/AKT pathway, IL6/JAK2/STAT3 pathway, and YAP pathway are currently major research topics in BM studies.[11–13] However, due to the limitations of these techniques in cell classification, there is still significant room for further investigation. The emergence of single-cell sequencing technology can be well used to explore different types of cells and simulate the evolutionary process of epithelial cells (ECs). This allows our research to focus on the key stages of metastasis, thereby discovering more meaningful cells and driver genes, especially for tumor ECs which play a dominant role in the occurrence of BM in LUAD. Yuan et al. reported that loss of AMPKa2 was associated with BM in an immune-deficiency NF1-mutant melanoma model.[14] Additionally, Wu et al. also found that the circKIF4A-miR-637-STAT3 axis promotes the BM.[15] Both studies have demonstrated that the biological behavior of tumor cell is a considerable factor in BM. Therefore, depicting the characteristics of tumor cells would be important in understanding BM. Wang et al. utilized single-cell RNA data to identify BM-associated epithelial cells (BMAECs) and their biomarker, S100A9.[16] However, relevant studies are rare, and more profound studies should be performed to uncover the molecular mechanism of BM development.

The focus of our study was on the roles of ECs in BM from LUAD. By analyzing single-cell RNA (scRNA) sequencing data from pLUAD, BM and lymph node metastasis (LNM) samples, we have discovered a population of BMAECs expressing SPP1, SAA1, and CDKN2A, and it has been observed that this population is mainly composed of aneuploid cells from pLUAD, playing a crucial role in BM. To facilitate clinical

[1]Department of Integrated Traditional Chinese and Western Medicine, Shanghai Pulmonary Hospital, School of Medicine, Tongji University, Shanghai, China
[2]Graduate School of Shanghai University of Traditional Chinese Medicine, Shanghai, China
[3]Department of Thoracic Surgery, Shanghai Pulmonary Hospital, School of Medicine, Tongji University, Shanghai, China
[4]Department of Radiation Oncology, Shanghai Pulmonary Hospital, School of Medicine, Tongji University, Shanghai, China
[5]These authors contributed equally
[6]Lead contact
*Correspondence: dr_caoy@aliyun.com (Y.C.), 1701005@tongji.edu.cn (L.W.), songxiao198327@163.com (X.S.)
https://doi.org/10.1016/j.isci.2024.109258

application, we identified, as markers for BMAECs. Our study concluded that both LNM and BM in LUAD originated from pLUAD lesions, but there is currently insufficient evidence to prove a direct association between BM lesions and LNM lesions, which provides inspiration for further investigation of the tumor microenvironment (TME) in BM.

RESULTS

ScRNA sequencing reveals different cellular composition and immune microenvironment in pLUAD BM and LNM samples

The overall workflow of the present study is displayed in Figure 1A. After performing quality control, data normalization, and principal component analysis on scRNA-seq data, the cells of pLUAD BM and LNM samples were subjected to overall dimensionality reduction clustering (Figure 1B) and separate clustering using the UMAP algorithm. Then, cells from pLUAD BM and LNM samples were automatically and manually annotated by 12 types of known cell lineages (Figures 1C–1E). 32,912 cells from the pLUAD sample, 16,032 cells from the BM sample and 16,751 cells from the LNM sample were retained for further analysis. T cells, B cells, macrophages, NK cells, and ECs are present at higher proportions in pLUAD BM and LNM samples (Figures 1F–1H). However, ECs were the most abundant cells in BM (33.6%), which was different from that in pLUAD (6.5%) and LNM (7.0%). Generally, the cellular constitutions in LUAD primary and metastatic samples were totally different (Figure 1I).

Cell–Cell Communication analysis

As shown in Figures 2A–2C, according to our analysis results, the interaction net number of ECs in the BM samples signaling pathway has decreased. The primary group accounts for 14.4%, the LNM group accounts for 18.5%, while the BM group accounts for 10.3%. Interestingly, the signaling pathways associated with ECs were unchanged significantly, including the GDF, EGF, SPP1 and VEGF pathways that are highly associated with tumor growth and metastasis (Table S1).

Aneuploid ECs was identified in the pLUAD BM and LNM samples

We next investigated populations of ECs. CopyKAT can further cluster tumor cells and identify different subsets. CopyKAT does not need normal cells as a reference and can automatically find diploid cells as normal cells, making up for the shortcomings of inferCNV and HoneyBadger. We first re-clustered the ECs (Figures 2D–2F) and separated aneuploid and diploid cells using the CopyKAT algorithm based on copy number variations (CNVs) in Figures 2G–2I. The aneuploid ECs in pLUAD are primarily concentrated in cluster 2, 3, 4, 6, 7, 8, and 11 and are mainly concentrated in cluster 0 and 10 in BM. Almost all cells of the cluster 0 and 1 in ECs of LNM consist of aneuploid cells.

Cellular origins and driver genes of BMAECs analysis

We integrated pLUAD and BM ECs, reclustered them (Figure 3A), and simulated the evolution and metastasis of ECs using pseudotime analysis (Figure 3B). ECs in clusters 9, 11, 14, and 18 are located at pivotal positions where pLUAD evolves into BM. Therefore, we define the groups of cells as BMAECs. Interestingly, we found that clusters 14 and 18 are almost entirely composed of aneuploid ECs from pLUAD. Using the same method, we reanalyzed the pLUAD and LNM ECs and defined the ECs in clusters 4, 5, 9, and 10 as LNM-associated epithelial cells (LNMAECs) in Figures 3C and 3D. Among them, clusters 5, 9, and 10 are predominantly composed of aneuploid ECs from pLUAD. This suggests that aneuploid ECs of LUAD are closely associated with the metastasis and prognosis of tumors.

As shown in the Figures 4A and 4B, we further explored the evolutionary relationship between pLUAD ECs, BMAECs, and LNMAECs by performing clustering and pseudotime analysis. The results indicate that both BMAECs and LNMAECs are derived from pLUAD ECs. However, our study does not provide evidence of a direct relationship between BMAECs and LNM lesions.

We performed KEGG enrichment analysis using differentially expressed genes in BMAECs and found that the highly expressed genes in BMAECs are mainly enriched in pathways related to cell adhesion molecules, focal adhesion, and transcriptional misregulation in cancer, which are associated with tumor metastasis (Figure 4C). We extracted the top 50 genes ranked in BMAECs and found that SPP1 SAA1 and CDKN2A are specifically expressed in cluster 9, 11, 14, and 18 (Figure 4D). This suggests that the markers (SPP1 SAA1 and CDKN2A) may serve as predictive genes for brain metastasis (Figures 4E–4G).

Validation of BM driver genes in LUAD associated with metastasis and prognosis

To verify the significance of BMAECs involvement in BM, we performed IHC staining of BMAECs markers (SPP1 SAA1 and CDKN2A) in the 26 pLUAD samples and 20 pLUAD patients with brain metastasis (Figure 5A). Compared with the pLUAD patients without brain metastasis, the expression of BMAECs markers were significantly higher in the pLUAD patients with brain metastasis and H-scores are shown in Figures 5B–5D ($p = 0.0002$, $p = 0.0272$, $p = 0.0201$, respectively). As shown in the Figures 5E–5G, according to Kaplan-Meier estimation analysis, high expression of BMAECs markers predicted a higher probability of BM in patients (log rank $p < 0.0001$, $p = 0.0230$, $p = 0.0180$, respectively).

In order to validate the importance of BMAECs' participation in BM, we performed Multiplex IF staining of markers of BMAECs (SPP1 SAA1 and CDKN2A) in the pLUAD samples, and pLUAD patients with brain metastasis (Figure 5H). Compared with the pLUAD patients without brain metastasis, the cell proportions of BMAECs with the three marker genes coexpression were significantly higher in the pLUAD patients with BM. Altogether, these findings suggest that BMAECs has an apparently higher abundance in pLUAD samples with future BM, and the expression of SPP1, SAA1, and CDKN2A may be a key predictor of BM in LUAD.

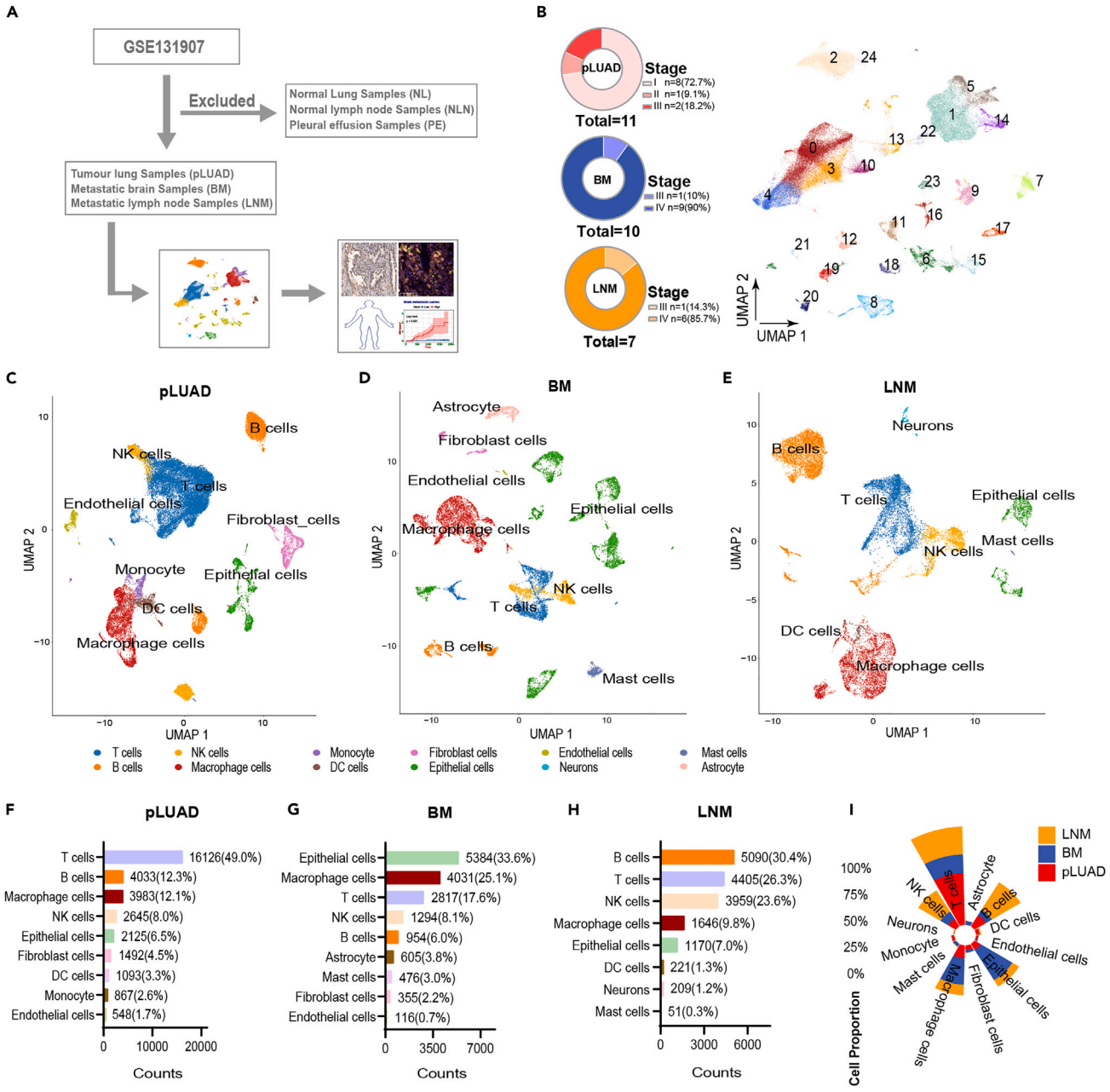

Figure 1. Proportion of different cellular infiltrations in pLUAD BM and LNM samples delineated by scRNA-seq analysis

(A) Overall workflow of the present study.

(B–H) (B) Overall dimensionality reduction clustering of the three samples. The main cell types annotated by known cell lineages in pLUAD (C) BM (D) and LNM (E) samples are illustrated by UMAP plots. Bar charts illustrates the comparison of the proportions of major cell types in samples (F) pLUAD (G) BM and (H) LNM. (I) Comparison of the proportions of the main cell types between the pLUAD BM and LNM samples is displayed by the proportion plot.

DISCUSSION

The primary causes of BM, as reported, include the distinctive genetic subtypes of pLUAD, alterations in transcriptional and epigenetic patterns in pLUAD cells, and TME within the brain that facilitates BM. The role of special cells within the central nervous system (CNS), including astrocytes and microglia, as well as the interactions between various immune cells and cancer cells, has become a research hotspot. According to reports, microglia and macrophages play an indirect tumor-supportive role in brain metastasis, which is related to the settlement of tumor cells in the intracranial space.[17] In our study, the significant increase in infiltration of macrophages indirectly suggests the role of macrophages in promoting the colonization of tumor cells in the brain during the process of BM. Wang et al. demonstrates that the quantity of

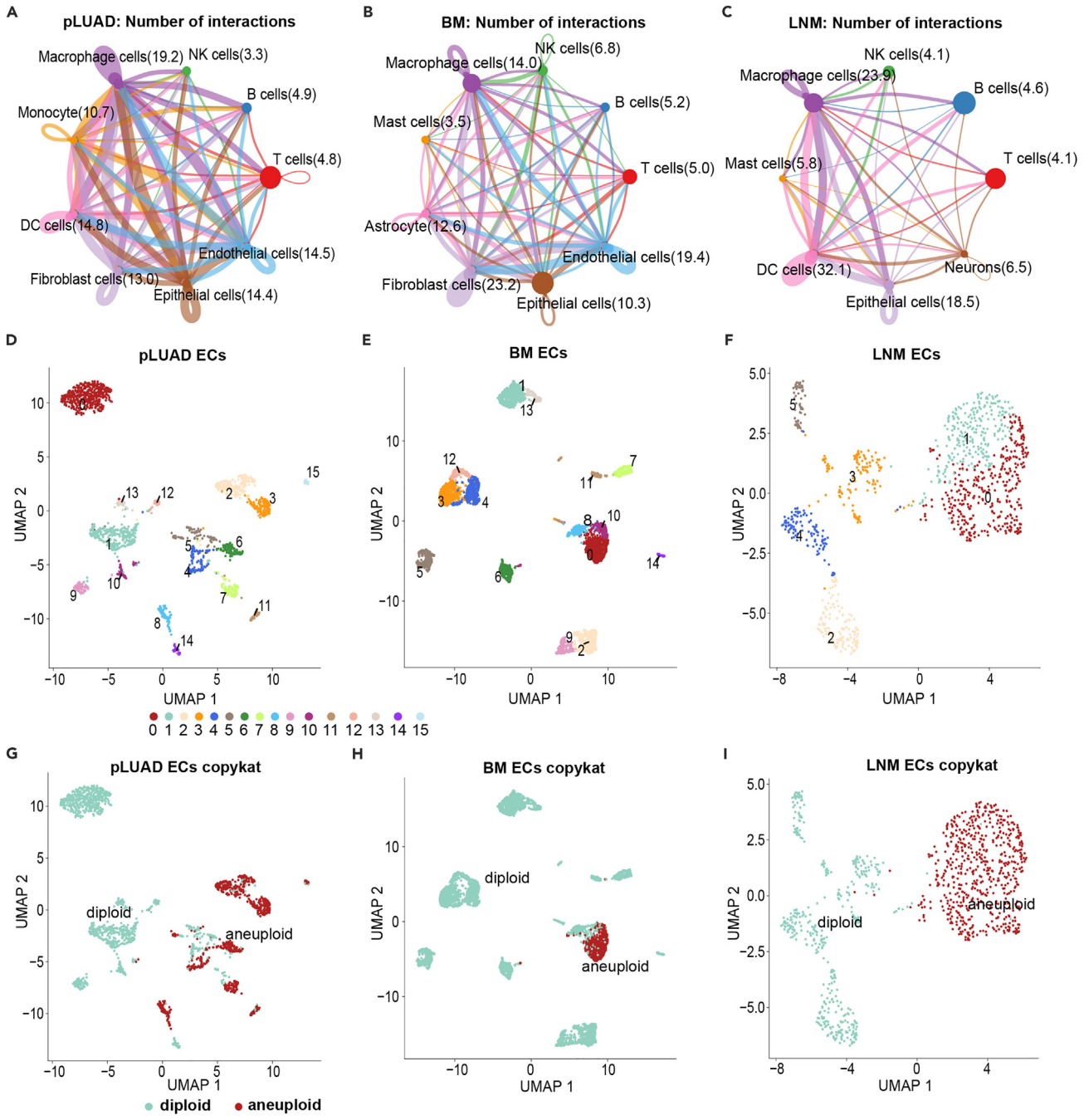

Figure 2. Cell–cell communication and aneuploid ECs analysis

The Cell Communication of (A) pLUAD (B) BM and (C) LNM samples are illustrated by circle diagram. The ECs of (D) pLUAD (E) BM and (F) LNM are re-clustered by UMAP plots. The CopyKAT algorithm based on copy number variation is utilized to identify aneuploid and diploid cells in (G) pLUAD (H) BM and (I) LNM.

$CD8^+$ T cells in brain metastasis (BM) tissue is significantly lower than in primary tumor tissue.[16] Consistently, using the similar approach, a recent study found BM lesions exhibited lower T cell infiltration in compare to the primary tumors.[18] Low-intensity pulsed ultrasound (LIPU) is a safe treatment method that can temporarily disrupt the blood-brain barrier (BBB), thereby enhancing the delivery of chemotherapy drugs to tumors and immune cell infiltration.[19] Our study indicates that the infiltration of T cells in BM (17.6%) lesions is significantly reduced compared to the pLUAD (49.0%) lesions. This suggests that the brain metastasis TME and blood-brain barrier influence immune cell infiltration and may also have an impact on the isolation of T cells. How to break through the blood-brain barrier to increase T cell immune infiltration may become an important research direction for the treatment of BM in the future.

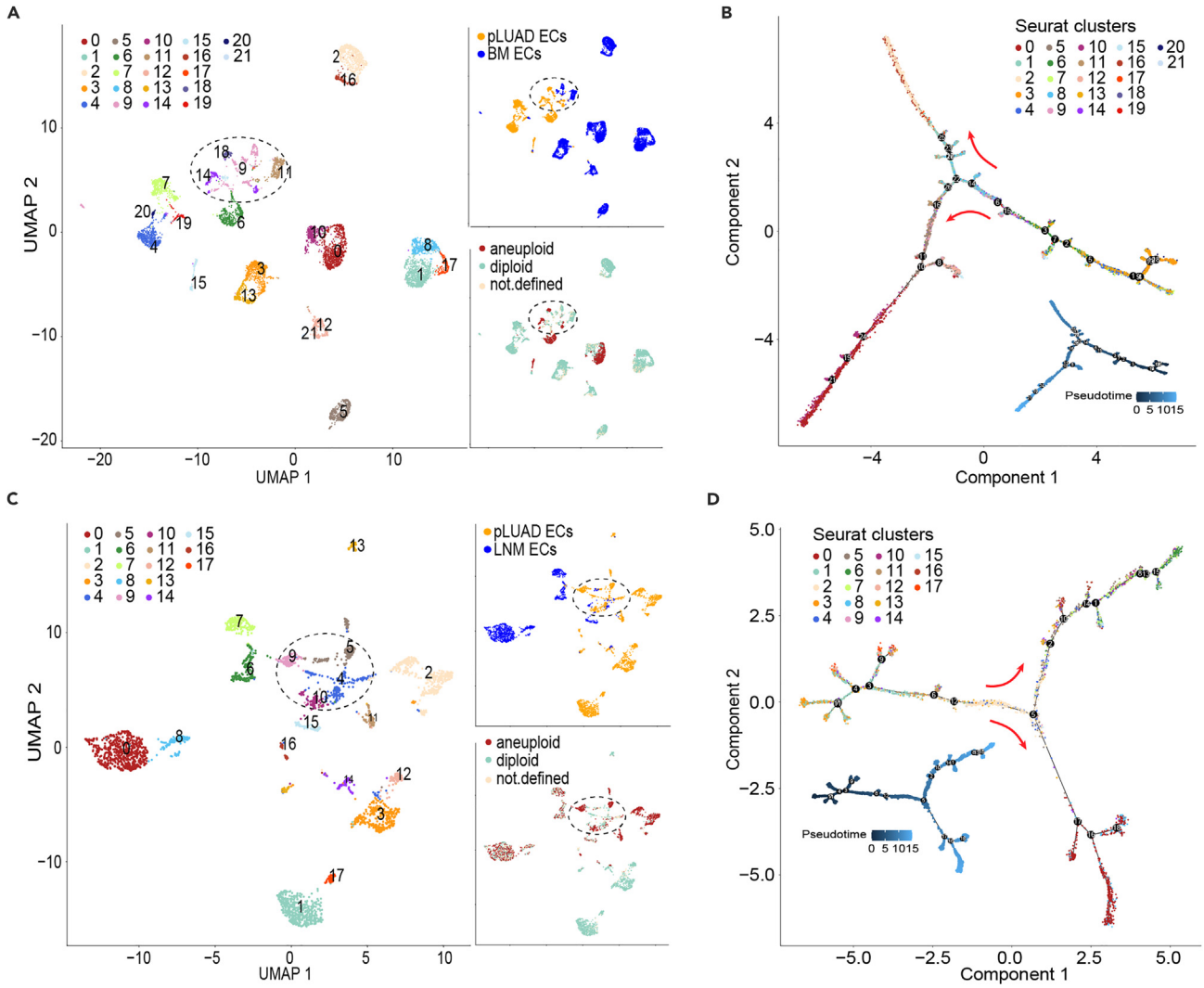

Figure 3. The origin of metastasis-associated ECs analysis

(A) ECs reclustering of pLUAD merged BM samples.

(B) Pseudotime trajectory analysis of BMAECs from LUAD.

(C) ECs reclustering of pLUAD merged LNM samples.

(D) Pseudotime trajectory analysis of LNMAECs from LUAD.

In our study, we found that the infiltration ratio of ECs in BM (33.6%) was significantly higher than that in primary lesions (6.5%) and LNM (7.0%). Cell communication analysis also demonstrated that tumor ECs predominantly act on pathways promoting tumor metastasis, such as EGF and VEGF. Liu et al. effectively blocked cell aggregation *in vitro* and reduced lung metastasis *in vivo* by blocking EGFR using a novel anti-EGFR monoclonal antibody (clone LA1).[20] Many studies have similarly shown that tumor ECs play an important role in tumor growth, evolution, and metastasis.

Our study identified a subgroup of cells which may be the cellular origin of BM from LUAD. Interestingly, most of these cells consisted of aneuploid cells. Recent studies suggest that aneuploidy is a context-dependent, cancer-type-specific oncogenic event that may have clinical relevance as a prognostic marker and as a potential therapeutic target.[21] Andrew et al. showed that aneuploid cells are more malignant and promote tumor growth and metastasis.[22] Our study showed that aneuploid cell populations were mainly enriched in cell adhesion pathway, transcriptional dysregulation pathway, TNF signaling pathway, which further suggests that aneuploid cells are strongly associated with LUAD metastasis. We identified biomarkers for these cells (SPP1, SAA1, and CDKN2A). As reported, SPP1 promotes cancer cell survival and regulates tumor-associated angiogenesis and inflammation.[23] SAA1 is able to activate MAPK/IκB/NF-κB signaling and promote tumor cell invasion and migration *in vitro* and *in vivo*.[24] Alterations in genes encoding the CDK4/CCND1, CDKN2A/2B, and PI3K signaling pathways are enriched in BM, suggesting that they are associated with an increased risk of metastasis.[25] Our study also

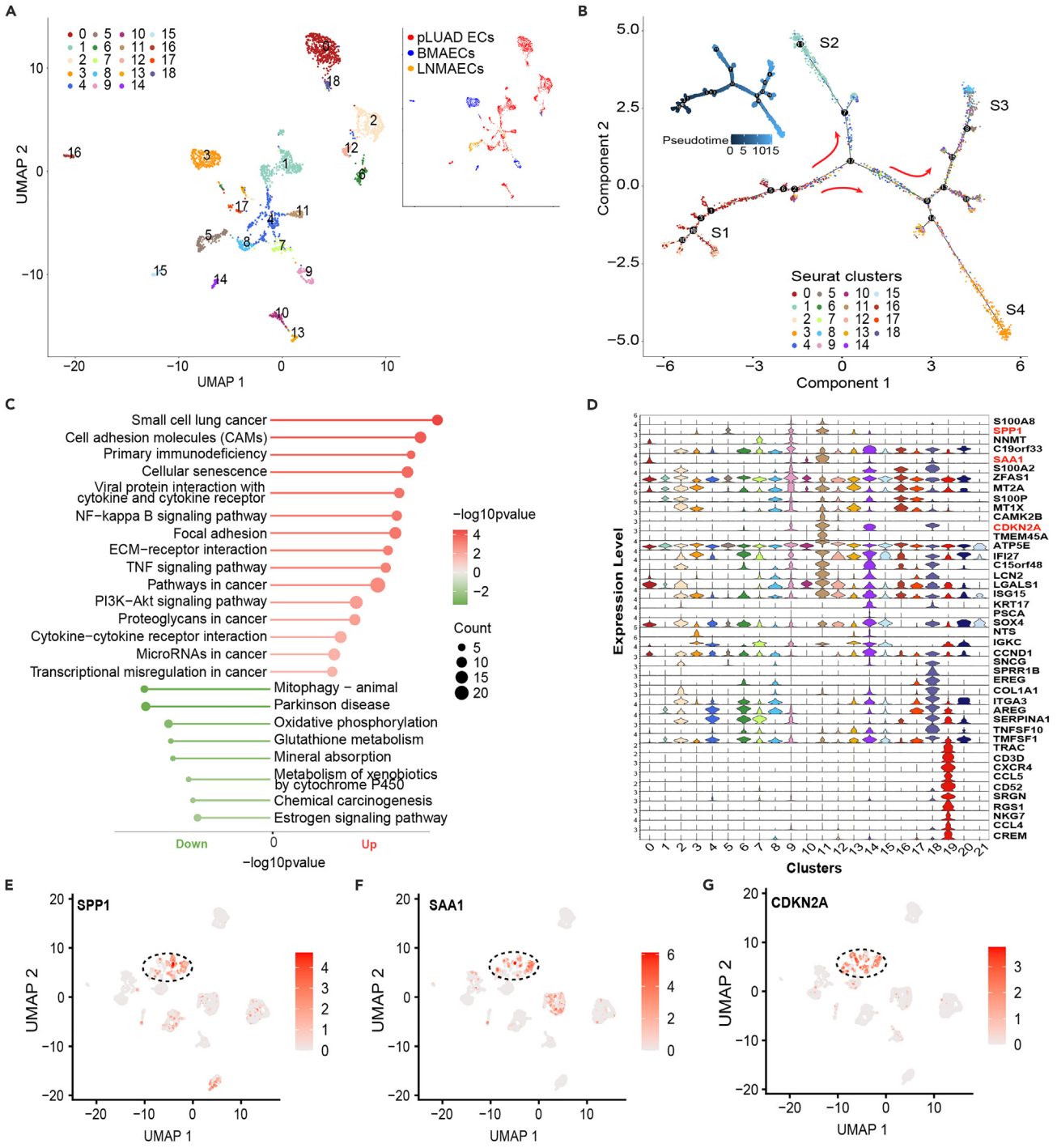

Figure 4. Driver genes of BMAECs analysis

Metastasis-associated ECs (A) reclustering analysis and (B) pseudotime trajectory analysis.

(C) KEGG enrichment analysis of BMAECs.

(D) Specific gene display of BMAECs. SPP1 (E) SAA1 (F) and CDKN2A (G) expression intensity in BMAECs.

addressed the shortcomings of previous research by verifying the specificity of these biomarkers using samples from Shanghai Pulmonary Hospital, including pLUAD patients with BM and pLUAD patients without BM, providing clinically significant results. While the function of these biomarkers is pivotal in BM, the entire ecosystem of metastasis sites is also important. Zou et al. also depicted that the microenvironment in liver and brain metastasis of breast cancer was consistently immunosuppressive via single-cell sequencing even though the

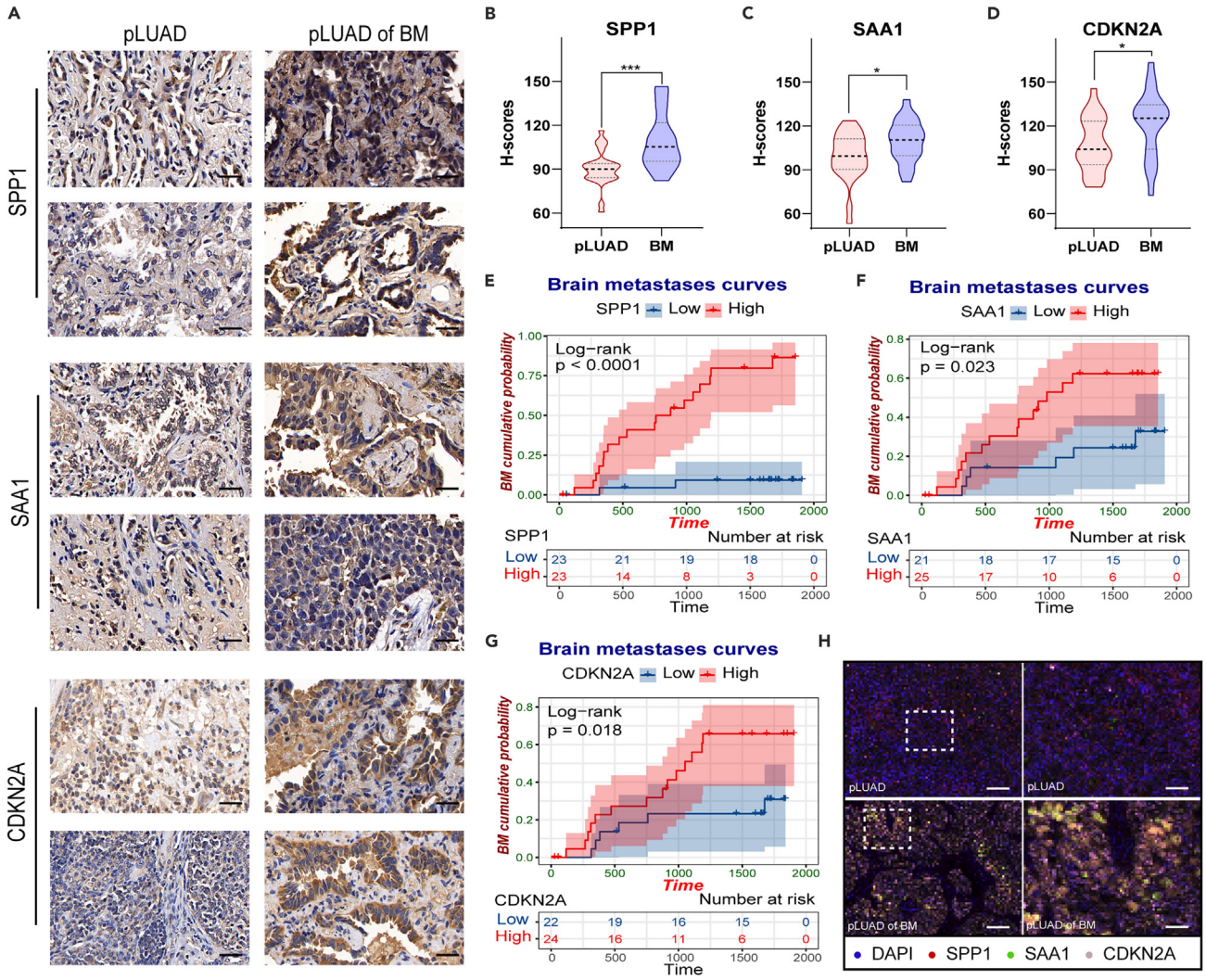

Figure 5. Validation of BM driver genes in LUAD associated with metastasis and prognosis

(A) Representative IHC staining plots of SPP1, SAA1, and CDKN2A in samples of pLUAD (left panel), pLUAD of BM (right panel). Cell nuclei were counterstained with DAPI (blue). Scale bar: 5 μm.

(B) SPP1 (C) SAA1 and (D) CDKN2A H-scores are represented by bar graphs. * indicates $p < 0.05$, ** indicates $p < 0.01$, and *** indicates $p < 0.001$. BM cumulative probability curves are shown in (E) (F) and (G) plots (log rank $p < 0.0001$, $p = 0.0230$, $p = 0.0180$, respectively).

(H) Representative IF confocal staining plots for markers SPP1 (red), SAA1 (green), CDKN2A (pink) in pLUAD (top) and BM (bottom) samples. Cell nuclei were counterstained with DAPI (blue). Scale bar: 80 μm (left panel), 20 μm (right panel).

tumors were heterogeneous. This demonstrated that different signals might be determinants of metastasis sites, but the ecosystem could imperceptibly affect the process of distant colonization.[26]

In conclusion, our study involved analyzing scRNA-seq data and identified a cell subset called BMAECs, which consists of mostly aneuploid cells and potentially represents the cellular origin of BM. We also discovered potential biomarkers (SPP1, SAA1 and CDKN2A) associated with BMAECs. We then validated these findings using clinical samples. These findings may have implications for more accurate early identification of high-risk patients for metastasis and the development of targeted therapies in the future.

Limitations of the study

The scRNA-seq data were retrieved from online database, which makes it vulnerable to inherent shortcomings. Consequently, this study has several limitations. Firstly, we have screened the data published online in the GEO database.[27] Unfortunately, we did not find any available data other than GSE131907,[28] which has resulted in limited sample size and potential sample selection bias. Therefore, to enhance the robustness of our conclusion, we validated the conclusion in our patient's cohort. Secondly, in real-world setting, the initiation of BM is a complex process, thereinto, involving not only the aggressive biological behavior of tumor cells, but also the intricate interactions among tumor cells,

mesenchymal stromal cells, and immune cells. Additionally, the different cluster within BMAECs (i.e., cluster 9, 11, 14, and 18) might play different roles in this process. However, it is challenging to further elucidate these interplays within the biological process based on our data, and further studies focusing on this aspect would be expected. Lastly, out of an interpretation of BMAECs, the cluster 9 and 11 exhibit similar expression pattern, which might result from genetic and epigenetic reprogramming processes. Nevertheless, we still face difficulties in exploring the upstream factors.

STAR★METHODS

Detailed methods are provided in the online version of this paper and include the following:

- KEY RESOURCES TABLE
- RESOURCE AVAILABILITY
  - Lead contact
  - Materials availability
  - Data and code availability
- EXPERIMENTAL MODEL AND SUBJECT DETAILS
- METHOD DETAILS
  - Data source of patients
  - Processing of scRNA data and cell type annotations
  - Cell–cell interaction analysis
  - Gene functional enrichment analysis
  - Immunohistochemistry (IHC) staining and quantification
  - Copy number variation estimation
  - Pseudotime trajectory analysis of tumor ECs
  - Multiplex immunofluorescence (mIF) staining
- QUANTIFICATION AND STATISTICAL ANALYSIS

SUPPLEMENTAL INFORMATION

Supplemental information can be found online at https://doi.org/10.1016/j.isci.2024.109258.

ACKNOWLEDGMENTS

This research was financially supported by Shanghai Administration of Traditional Chinese Medicine (ZY-FWTX-7001; ZY (2021-2023)-0302), Shanghai Science and Technology Committee (18401901500), Shanghai Shenkang Hospital Development Center (SHDC12018X20), and National Natural Science Foundation of China (No.82004115; No.82304968).

AUTHOR CONTRIBUTIONS

Y.W. and F.Y. conceived and designed the experiments, performed, analyzed and interpreted all data. S.L., X.L., Z.G., R.F., and Y.C. contributed reagents, materials, analysis tools or data and wrote the paper. L.W. and X.S. contributed reagents, materials, analysis tools or data. All authors read and approved the final manuscript.

DECLARATION OF INTERESTS

The authors declare no competing interests.

Received: October 17, 2023
Revised: January 16, 2024
Accepted: February 13, 2024
Published: February 16, 2024

REFERENCES

1. Nguyen, T.T., Lee, H.S., Burt, B.M., Wu, J., Zhang, J., Amos, C.I., and Cheng, C. (2022). A lepidic gene signature predicts patient prognosis and sensitivity to immunotherapy in lung adenocarcinoma. Genome Med. *14*, 5. https://doi.org/10.1186/s13073-021-01010-w.
2. Cagney, D.N., Martin, A.M., Catalano, P.J., Redig, A.J., Lin, N.U., Lee, E.Q., Wen, P.Y., Dunn, I.F., Bi, W.L., Weiss, S.E., et al. (2017). Incidence and prognosis of patients with brain metastases at diagnosis of systemic malignancy: a population-based study. Neuro Oncol. *19*, 1511–1521. https://doi.org/10.1093/neuonc/nox077.
3. Boire, A., Brastianos, P.K., Garzia, L., and Valiente, M. (2020). Brain metastasis. Nat. Rev. Cancer *20*, 4–11. https://doi.org/10.1038/s41568-019-0220-y.
4. Wang, H., Deng, Q., Lv, Z., Ling, Y., Hou, X., Chen, Z., Dinglin, X., Ma, S., Li, D., Wu, Y., et al. (2019). N6-methyladenosine induced miR-143-3p promotes the brain metastasis of lung cancer via regulation of VASH1. Mol. Cancer *18*, 181. https://doi.org/10.1186/s12943-019-1108-x.

5. Shih, D.J.H., Nayyar, N., Bihun, I., Dagogo-Jack, I., Gill, C.M., Aquilanti, E., Bertalan, M., Kaplan, A., D'Andrea, M.R., Chukwueke, U., et al. (2020). Genomic characterization of human brain metastases identifies drivers of metastatic lung adenocarcinoma. Nat. Genet. *52*, 371–377. https://doi.org/10.1038/s41588-020-0592-7.
6. Cheng, Y.J., Fan, F., Zhang, Z., and Zhang, H.J. (2023). Lipid metabolism in malignant tumor brain metastasis: reprogramming and therapeutic potential. Expert Opin. Ther. Targets *27*, 861–878. https://doi.org/10.1080/14728222.2023.2255377.
7. Wang, Y., Ye, F., Liang, Y., and Yang, Q. (2021). Breast cancer brain metastasis: insight into molecular mechanisms and therapeutic strategies. Br. J. Cancer *125*, 1056–1067. https://doi.org/10.1038/s41416-021-01424-8.
8. Galldiks, N., Kocher, M., Ceccon, G., Werner, J.M., Brunn, A., Deckert, M., Pope, W.B., Soffietti, R., Le Rhun, E., Weller, M., et al. (2020). Imaging challenges of immunotherapy and targeted therapy in patients with brain metastases: response, progression, and pseudoprogression. Neuro Oncol. *22*, 17–30. https://doi.org/10.1093/neuonc/noz147.
9. Singh, M., Venugopal, C., Tokar, T., Brown, K.R., McFarlane, N., Bakhshinyan, D., Vijayakumar, T., Manoranjan, B., Mahendram, S., Vora, P., et al. (2017). RNAi screen identifies essential regulators of human brain metastasis-initiating cells. Acta Neuropathol. *134*, 923–940. https://doi.org/10.1007/s00401-017-1757-z.
10. Fukumura, K., Malgulwar, P.B., Fischer, G.M., Hu, X., Mao, X., Song, X., Hernandez, S.D., Zhang, X.H.F., Zhang, J., Parra, E.R., et al. (2021). Multi-omic molecular profiling reveals potentially targetable abnormalities shared across multiple histologies of brain metastasis. Acta Neuropathol. *141*, 303–321. https://doi.org/10.1007/s00401-020-02256-1.
11. Jin, Y., Kang, Y., Wang, M., Wu, B., Su, B., Yin, H., Tang, Y., Li, Q., Wei, W., Mei, Q., et al. (2022). Targeting polarized phenotype of microglia via IL6/JAK2/STAT3 signaling to reduce NSCLC brain metastasis. Signal Transduct. Targeted Ther. *7*, 52. https://doi.org/10.1038/s41392-022-00872-9.
12. Wei, C., Dong, X., Lu, H., Tong, F., Chen, L., Zhang, R., Dong, J., Hu, Y., Wu, G., and Dong, X. (2019). LPCAT1 promotes brain metastasis of lung adenocarcinoma by up-regulating PI3K/AKT/MYC pathway. J. Exp. Clin. Cancer Res. *38*, 95. https://doi.org/10.1186/s13046-019-1092-4.
13. Li, C., Zheng, H., Xiong, J., Huang, Y., Li, H., Jin, H., Ai, S., Wang, Y., Su, T., Sun, G., et al. (2022). miR-596-3p suppresses brain metastasis of non-small cell lung cancer by modulating YAP1 and IL-8. Cell Death Dis. *13*, 699. https://doi.org/10.1038/s41419-022-05062-7.
14. Yuan, P., Teng, D., de Groot, E., Li, M., Trousil, S., Shen, C.H., Roszik, J., Davies, M.A., Gopal, Y.N.V., and Zheng, B. (2023). Loss of AMPKα2 promotes melanoma tumor growth and brain metastasis. iScience *26*, 106791. https://doi.org/10.1016/j.isci.2023.106791.
15. Wu, S., Lu, J., Zhu, H., Wu, F., Mo, Y., Xie, L., Song, C., Liu, L., Xie, X., Li, Y., et al. (2024). A novel axis of circKIF4A-miR-637-STAT3 promotes brain metastasis in triple-negative breast cancer. Cancer Lett. *581*, 216508. https://doi.org/10.1016/j.canlet.2023.216508.
16. Wang, Z., Wang, Y., Chang, M., Wang, Y., Liu, P., Wu, J., Wang, G., Tang, X., Hui, X., Liu, P., et al. (2023). Single-cell transcriptomic analyses provide insights into the cellular origins and drivers of brain metastasis from lung adenocarcinoma. Neuro Oncol. *25*, 1262–1274. https://doi.org/10.1093/neuonc/noad017.
17. Schulz, M., Salamero-Boix, A., Niesel, K., Alekseeva, T., and Sevenich, L. (2019). Microenvironmental Regulation of Tumor Progression and Therapeutic Response in Brain Metastasis. Front. Immunol. *10*, 1713. https://doi.org/10.3389/fimmu.2019.01713.
18. Jiang, T., Yan, Y., Zhou, K., Su, C., Ren, S., Li, N., Hou, L., Guo, X., Zhu, W., Zhang, H., et al. (2021). Characterization of evolution trajectory and immune profiling of brain metastasis in lung adenocarcinoma. npj Precis. Oncol. *5*, 6. https://doi.org/10.1038/s41698-021-00151-w.
19. Sabbagh, A., Beccaria, K., Ling, X., Marisetty, A., Ott, M., Caruso, H., Barton, E., Kong, L.Y., Fang, D., Latha, K., et al. (2021). Opening of the Blood-Brain Barrier Using Low-Intensity Pulsed Ultrasound Enhances Responses to Immunotherapy in Preclinical Glioma Models. Clin. Cancer Res. *27*, 4325–4337. https://doi.org/10.1158/1078-0432.Ccr-20-3760.
20. Liu, X., Adorno-Cruz, V., Chang, Y.F., Jia, Y., Kawaguchi, M., Dashzeveg, N.K., Taftaf, R., Ramos, E.K., Schuster, E.J., El-Shennawy, L., et al. (2021). EGFR inhibition blocks cancer stem cell clustering and lung metastasis of triple negative breast cancer. Theranostics *11*, 6632–6643. https://doi.org/10.7150/thno.57706.
21. Ben-David, U., and Amon, A. (2020). Context is everything: aneuploidy in cancer. Nat. Rev. Genet. *21*, 44–62. https://doi.org/10.1038/s41576-019-0171-x.
22. Holland, A.J., and Cleveland, D.W. (2012). Losing balance: the origin and impact of aneuploidy in cancer. EMBO Rep. *13*, 501–514. https://doi.org/10.1038/embor.2012.55.
23. Psallidas, I., Stathopoulos, G.T., Maniatis, N.A., Magkouta, S., Moschos, C., Karabela, S.P., Kollintza, A., Simoes, D.C.M., Kardara, M., Vassiliou, S., et al. (2013). Secreted phosphoprotein-1 directly provokes vascular leakage to foster malignant pleural effusion. Oncogene *32*, 528–535. https://doi.org/10.1038/onc.2012.57.
24. Zhang, Y., Wei, Y., Jiang, B., Chen, L., Bai, H., Zhu, X., Li, X., Zhang, H., Yang, Q., Ma, J., et al. (2017). Scavenger Receptor A1 Prevents Metastasis of Non-Small Cell Lung Cancer via Suppression of Macrophage Serum Amyloid A1. Cancer Res. *77*, 1586–1598. https://doi.org/10.1158/0008-5472.Can-16-1569.
25. Wang, H., Ou, Q., Li, D., Qin, T., Bao, H., Hou, X., Wang, K., Wang, F., Deng, Q., Liang, J., et al. (2019). Genes associated with increased brain metastasis risk in non-small cell lung cancer: Comprehensive genomic profiling of 61 resected brain metastases versus primary non-small cell lung cancer (Guangdong Association Study of Thoracic Oncology 1036). Cancer *125*, 3535–3544. https://doi.org/10.1002/cncr.32372.
26. Zou, Y., Ye, F., Kong, Y., Hu, X., Deng, X., Xie, J., Song, C., Ou, X., Wu, S., Wu, L., et al. (2023). The Single-Cell Landscape of Intratumoral Heterogeneity and The Immunosuppressive Microenvironment in Liver and Brain Metastases of Breast Cancer. Adv. Sci. *10*, e2203699. https://doi.org/10.1002/advs.202203699.
27. Barrett, T., Wilhite, S.E., Ledoux, P., Evangelista, C., Kim, I.F., Tomashevsky, M., Marshall, K.A., Phillippy, K.H., Sherman, P.M., Holko, M., et al. (2013). NCBI GEO: archive for functional genomics data sets–update. Nucleic Acids Res. *41*, D991–D995. https://doi.org/10.1093/nar/gks1193.
28. Kim, N., Kim, H.K., Lee, K., Hong, Y., Cho, J.H., Choi, J.W., Lee, J.I., Suh, Y.L., Ku, B.M., Eum, H.H., et al. (2020). Single-cell RNA sequencing demonstrates the molecular and cellular reprogramming of metastatic lung adenocarcinoma. Nat. Commun. *11*, 2285. https://doi.org/10.1038/s41467-020-16164-1.
29. Satija, R., Farrell, J.A., Gennert, D., Schier, A.F., and Regev, A. (2015). Spatial reconstruction of single-cell gene expression data. Nat. Biotechnol. *33*, 495–502. https://doi.org/10.1038/nbt.3192.
30. Butler, A., Hoffman, P., Smibert, P., Papalexi, E., and Satija, R. (2018). Integrating single-cell transcriptomic data across different conditions, technologies, and species. Nat. Biotechnol. *36*, 411–420. https://doi.org/10.1038/nbt.4096.
31. Aran, D., Looney, A.P., Liu, L., Wu, E., Fong, V., Hsu, A., Chak, S., Naikawadi, R.P., Wolters, P.J., Abate, A.R., et al. (2019). Reference-based analysis of lung single-cell sequencing reveals a transitional profibrotic macrophage. Nat. Immunol. *20*, 163–172. https://doi.org/10.1038/s41590-018-0276-y.
32. Jin, S., Guerrero-Juarez, C.F., Zhang, L., Chang, I., Ramos, R., Kuan, C.H., Myung, P., Plikus, M.V., and Nie, Q. (2021). Inference and analysis of cell-cell communication using CellChat. Nat. Commun. *12*, 1088. https://doi.org/10.1038/s41467-021-21246-9.
33. Yu, G., Wang, L.G., Han, Y., and He, Q.Y. (2012). clusterProfiler: an R package for comparing biological themes among gene clusters. OMICS *16*, 284–287. https://doi.org/10.1089/omi.2011.0118.
34. Chiang, N., de la Rosa, X., Libreros, S., Pan, H., Dreyfuss, J.M., and Serhan, C.N. (2021). Cysteinyl-specialized proresolving mediators link resolution of infectious inflammation and tissue regeneration via TRAF3 activation. Proc. Natl. Acad. Sci. USA *118*, e2013374118. https://doi.org/10.1073/pnas.2013374118.
35. Cheng, Z., Vermeulen, M., Rollins-Green, M., DeVeale, B., and Babak, T. (2021). Cis-regulatory mutations with driver hallmarks in major cancers. iScience *24*, 102144. https://doi.org/10.1016/j.isci.2021.102144.
36. Tan, W.C.C., Nerurkar, S.N., Cai, H.Y., Ng, H.H.M., Wu, D., Wee, Y.T.F., Lim, J.C.T., Yeong, J., and Lim, T.K.H. (2020). Overview of multiplex immunohistochemistry/immunofluorescence techniques in the era of cancer immunotherapy. Cancer Commun. *40*, 135–153. https://doi.org/10.1002/cac2.12023.
37. Taylor, C.R., and Levenson, R.M. (2006). Quantification of immunohistochemistry–issues concerning methods, utility and semiquantitative assessment II. Histopathology *49*, 411–424. https://doi.org/10.1111/j.1365-2559.2006.02513.x.
38. Paschalis, A., Sheehan, B., Riisnaes, R., Rodrigues, D.N., Gurel, B., Bertan, C., Ferreira, A., Lambros, M.B.K., Seed, G., Yuan, W., et al. (2019). Prostate-specific Membrane Antigen Heterogeneity and DNA Repair Defects in Prostate Cancer. Eur. Urol. *76*, 469–478. https://doi.org/10.1016/j.eururo.2019.06.030.
39. Gao, R., Bai, S., Henderson, Y.C., Lin, Y., Schalck, A., Yan, Y., Kumar, T., Hu, M., Sei, E.,

Davis, A., et al. (2021). Delineating copy number and clonal substructure in human tumors from single-cell transcriptomes. Nat. Biotechnol. *39*, 599–608. https://doi.org/10.1038/s41587-020-00795-2.

40. Qiu, X., Mao, Q., Tang, Y., Wang, L., Chawla, R., Pliner, H.A., and Trapnell, C. (2017). Reversed graph embedding resolves complex single-cell trajectories. Nat. Methods *14*, 979–982. https://doi.org/10.1038/nmeth.4402.
41. Cao, J., Spielmann, M., Qiu, X., Huang, X., Ibrahim, D.M., Hill, A.J., Zhang, F., Mundlos, S., Christiansen, L., Steemers, F.J., et al. (2019). The single-cell transcriptional landscape of mammalian organogenesis. Nature *566*, 496–502. https://doi.org/10.1038/s41586-019-0969-x.
42. Taube, J.M., Akturk, G., Angelo, M., Engle, E.L., Gnjatic, S., Greenbaum, S., Greenwald, N.F., Hedvat, C.V., Hollmann, T.J., Juco, J., et al. (2020). The Society for Immunotherapy of Cancer statement on best practices for multiplex immunohistochemistry (IHC) and immunofluorescence (IF) staining and validation. J. Immunother. Cancer *8*, e000155. https://doi.org/10.1136/jitc-2019-000155.
43. Vetter, T.R., and Mascha, E.J. (2018). Unadjusted Bivariate Two-Group Comparisons: When Simpler is Better. Anesth. Analg. *126*, 338–342. https://doi.org/10.1213/ane.0000000000002636.
44. Schober, P., and Vetter, T.R. (2018). Survival Analysis and Interpretation of Time-to-Event Data: The Tortoise and the Hare. Anesth. Analg. *127*, 792–798. https://doi.org/10.1213/ane.0000000000003653.

STAR★METHODS

KEY RESOURCES TABLE

REAGENT or RESOURCE	SOURCE	IDENTIFIER
Antibodies		
Anti-SPP1 (IHC)	Proteintech	Cat# 22952-1-AP
Anti-SAA1 (IHC)	Zenbio	Cat# R381812
Anti-CDKN2A (IHC; mIF)	Proteintech	Cat# 10883-1-AP
Anti-SPP1 (mIF)	AiFang biological	Cat# AF03532
Anti-SAA1 (mIF)	AiFang biological	Cat# AF301253
Biological samples		
Paraffin section	Shanghai Pulmonary Hospital, School of Medicine, Tongji University	N/A
Deposited data		
Single-cell RNA sequencing data	GEO	GSE131907
Software and algorithms		
Seurat v4.3.0	Butler A et al.[29]	https://satijalab.org/seurat/
R 4.2.1	N/A	http://www.rstudios.co
SingleR v2.0.0	Aran D et al.[30]	https://github.com/dviraran/SingleR.
CellChat v1.4.0	Cell chat	http://www.cellchat.org/
KEGG	Sangerbox	http://sangerbox.com/home.html
Code	N/A	https://blog.csdn.net/KeYan_Go/article/details/135560412?spm=1001.2014.3001.5501.

RESOURCE AVAILABILITY

Lead contact

Further information and requests for resources should be directed to and will be fulfilled by the lead contact, Xiao Song (songxiao198327@163.com).

Materials availability

This study did not generate new unique reagents.

Data and code availability

All data reported in this paper will be shared by the lead contact upon reasonable request.
Software and code used in this study are referenced in their corresponding STAR Methods sections and also the key resources table.
Any additional information required to reanalyze the data reported in this paper is available from the lead contact upon reasonable request.

EXPERIMENTAL MODEL AND SUBJECT DETAILS

The 46 samples in this study were all obtained from Shanghai Pulmonary Hospital. They were from Asian patients who had undergone surgery and received a histopathological diagnosis of LUAD, including 26 non-recurrent samples and 20 samples with BM. This cohort included 26 males and 20 females with the median age at diagnosis of 62 (range 48-74) and were classified as TNM stages II-III. This research was approved by the Shanghai Pulmonary Hospital Ethical Review Board (No. K18-037).

METHOD DETAILS

Data source of patients

The scRNA expression profiles of 11 pLUAD samples, 10 BM samples and 7 LNM samples originated from GSE131907 by Kim et al. were sequenced by the Illumina HiSeq 2500.[28] The corresponding pLUAD and BM tumor samples were surgically resected without receiving any treatment. LNM tumor samples were obtained by bronchoscopic puncture. In addition, during postoperative 5-year-follow-up we conducted a retrospective analysis of 46 patients coming from Shanghai Pulmonary Hospital who underwent surgery and were histopathologically diagnosed with LUAD, including 26 non-recurrent samples and 20 samples with BM. The study was carried out in accordance with Declaration of Helsinki and was approved by the Institutional Ethics Committee of Shanghai Pulmonary Hospital.

Processing of scRNA data and cell type annotations

Seurat v4.3.0 package in R 4.2.1 was used for data processing and visualization.[29,30] Based on the highly variable genes (HVGs), principle component analysis (PCA) was performed to determine significant dimensions, termed by principle components (PCs). Uniform Manifold Approximation and Projection (UMAP) principal component analysis was performed to reduce data dimensionality, clustering, and SingleR v2.0.0 was used to annotate cell types.[31]

Cell–cell interaction analysis

In this study, CellChat (v1.4.0) software was used to deduce, examine, and depict intercellular communications within different cell subsets.[32] Seurat is employed for normalizing expression matrix to analyze the interactions between ligands and receptors. The list of established ligand-receptor pairs was acquired from CellChatDB, a database supported by literature that encompasses interactions observed in mice and humans. Initially, we determined overexpressed ligands or receptors in diverse cell types, followed by the estimation of communication probabilities. This was achieved by evaluating all ligand and receptor interactions linked to each signaling pathway.

Gene functional enrichment analysis

For gene set functional enrichment analysis, KEGG rest API (https://www.kegg.jp/kegg/rest/keggapi.html) was applied to obtain the latest gene annotations of KEGG Pathway as background. The R software package clusterProfiler v3.14.3 was used for enrichment analysis to obtain the gene set enrichment results.[33] Setting a minimum gene set of 5 and a maximum gene set of 5000, P value<0.05 and FDR<0.25 were considered statistically significant.[34,35]

Immunohistochemistry (IHC) staining and quantification

Immunohistochemistry assay was performed on 10% formalin fixed, paraffin-embedded (FFPE) sections (26 pLUADs and 20 pLUADs samples in which BM occurred).[36,37] The antibodies used in each samples were: anti-SPP1 (22952-1-AP, Proteintech, 1:200), anti-SAA1 (R381812, Zenbio, 1:200), anti-CDKN2A (10883-1-AP, Proteintech, 1:500) and secondary antibody. The images of immunohistochemistry were recorded by a Panoramic MIDI digital slide scanner (3D HISTECH) and were analyzed by Quant Center2.1. The H-Score was defined as follows: H-Score (H-SCORE=$\sum$(PI×I)=(percentage of cells of weak intensity×1) + (percentage of cells of moderate intensity×2) + percentage of cells of strong intensity×3).[38]

Copy number variation estimation

To further explore the tumor epithelial cell subpopulations in LUAD, all ECs in scRNA data were extracted. Aneuploid chromosome ECs were identified using Copykat v1.1.0 package, and epithelial cells were reclustered to obtain subsets of aneuploid and diploid tumor cell subtype.[39]

Pseudotime trajectory analysis of tumor ECs

Monocle v2.10.1 was applied to construct pseudotime trajectory based on the gene expression profiles of tumor ECs.[40,41] After dimensionality reduction and cell ordering, all tumor ECs were projected and ordered into a trajectory with different branches, and the cells within the same branch were considered to own the same cellular state. Branched expression analysis modeling (BEAM) was further performed to identify the genes with branch-dependent expression patterns. These branch-dependent genes can help explore the mechanisms by which the cell fate decision is made.

Multiplex immunofluorescence (mIF) staining

mIF was performed on 10% FFPE sections by using Opal Multiplex IHC kit (NEL871001KT, Akoya Biosciences).[42]The samples were labeled with all four markers, including anti-SPP1 (AF03532, AiFang biological, 1:200), anti-SAA1 (AF301253, AiFang biological, 1:200), anti-CDKN2A (10883-1-AP, Proteintech, 1:500) and spectral DAPI at a 1:5 dilution. Multiplex IF staining was performed to clarify the proportion of positive cells co-expressing SPP1, SAA1, and CDKN2A.

QUANTIFICATION AND STATISTICAL ANALYSIS

Data were presented as mean ± SD. The statistical differences were assessed with Student's T-test. The Mann–Whitney U test was applied to compare categorical variables and nonnormally distributed variables between 2 groups.[43] Brain metastasis hazard curves were assessed with the Kaplan-Meier estimation analysis and the log-rank test.[44] The statistical analyses in this study were performed by R 4.0.5 software, and A two-tailed P value < 0.05 was considered statistically significant.